ornl

OAK RIDGE NATIONAL LABORATORY

UNION CARBIDE

NUREG/CR-1296
ORNL/NUREG/TM-376

LMFBR Aerosol Release and Transport Program Quarterly Progress Report for July-September 1979

T. S. Kress

Prepared for the U.S. Nuclear Regulatory Commission
Office of Nuclear Regulatory Research
Under Interagency Agreements DOE 40-551-75 and 40-552-75

OPERATED BY
UNION CARBIDE CORPORATION
FOR THE UNITED STATES
DEPARTMENT OF ENERGY

Printed in the United States of America. Available from
National Technical Information Service
U.S. Department of Commerce
5285 Port Royal Road, Springfield, Virginia 22161

Available from

GPO Sales Program
Division of Technical Information and Document Control
U.S. Nuclear Regulatory Commission
Washington, D.C. 20555

NUREG/CR-1296
ORNL/NUREG/TM-376
Dist. Category R7

Contract No. W-7405-eng-26

Engineering Technology Division

LMFBR AEROSOL RELEASE AND TRANSPORT PROGRAM QUARTERLY PROGRESS REPORT FOR JULY–SEPTEMBER 1979

T. S. Kress

Manuscript Completed – March 18, 1980
Date Published – April 1980

Prepared for the
U.S. Nuclear Regulatory Commission
Office of Nuclear Regulatory Research
Under Interagency Agreements DOE 40-551-75 and 40-552-75

NRC FIN No. B0121

Prepared by the
OAK RIDGE NATIONAL LABORATORY
Oak Ridge, Tennessee 37830
operated by
UNION CARBIDE CORPORATION
for the
DEPARTMENT OF ENERGY

NUREG/CR-1296
ORNL/NUREG/TM-376
Dist. Category R7

Contract No. W-7405-eng-26

Engineering Technology Division

LMFBR AEROSOL RELEASE AND TRANSPORT PROGRAM QUARTERLY PROGRESS REPORT FOR JULY–SEPTEMBER 197

T. S. Kress

Manuscript Completed – March 18, 1980
Date Published – April 1980

Prepared for the
U.S. Nuclear Regulatory Commission
Office of Nuclear Regulatory Research
Under Interagency Agreements DOE 40-551-75 and 40-552-75

NRC FIN No. B0121

Prepared by the
OAK RIDGE NATIONAL LABORATORY
Oak Ridge, Tennessee 37830
operated by
UNION CARBIDE CORPORATION
for the
DEPARTMENT OF ENERGY

CONTENTS

FOREWORD

This report summarizes progress under the Liquid-Metal Fast Breeder Reactor (LMFBR) Aerosol Release and Transport (ART) Program [sponsored by the Division of Reactor Safety Research of the Nuclear Regulatory Commission (NRC)] for the period July–September 1979.

Work on this program was initially reported as Volume III of a four-volume series entitled *Quarterly Progress Report on Reactor Safety Programs Sponsored by the NRC Division of Reactor Safety Research*. Prior reports of this series are

Report No.	Period covered
ORNL/TM-4655	April–June 1974
ORNL/TM-4729	July–September 1974
ORNL/TM-4805	October–December 1974
ORNL/TM-4914	January–March 1975
ORNL/TM-5021	April–June 1975

Beginning with the report covering the period July–September 1975, work under this program is now being reported as *LMFBR Aerosol Release and Transport Program Quarterly Progress Report*. Prior reports under this title are

Report No.	Period covered
ORNL/NUREG/TM-8	July–September 1975
ORNL/NUREG/TM-9	October–December 1975
ORNL/NUREG/TM-35	January–March 1976
ORNL/NUREG/TM-59	April–June 1976
ORNL/NUREG/TM-75	July–September 1976
ORNL/NUREG/TM-90	October–December 1976
ORNL/NUREG/TM-113	January–March 1977
ORNL/NUREG/TM-142	April–June 1977
ORNL/NUREG/TM-173	July–September 1977
ORNL/NUREG/TM-193	October–December 1977
ORNL/NUREG/TM-213	January–March 1978
ORNL/NUREG/TM-244	April–June 1978
ORNL/NUREG/TM-276	July–September 1978
ORNL/NUREG/TM-318	October–December 1978
ORNL/NUREG/TM-329	January–March 1979
ORNL/NUREG/TM-354	April–June 1979

Copies of all these reports are available from the Technical Information Center, Oak Ridge, Tennessee 37830.

SUMMARY

T. S. Kress

The Aerosol Release and Transport (ART) from the Liquid-Metal Fast Breeder Reactor (LMFBR) Fuel Program at Oak Ridge National Laboratory (ORNL) is designed to investigate the release, transport, and behavior of radionuclides originating from a hypothetical core-disruptive accident (HCDA) in an LMFBR. The experimental program is being conducted in the Fuel Aerosol Simulant Test (FAST) facility, the Nuclear Safety Pilot Plant (NSPP) facility, and the Containment Research Installation-II (CRI-II) facility. The analytical effort is designed to (1) support the experiments and (2) provide an independent assessment of the safety margins that exist for assessment of the radiological consequences of an HCDA.

During this reporting period, 13 tests were performed in the FAST facility, including seven tests in the FAST vessel and six tests in the CRI-III vessel, which is part of the FAST facility.

The seven FAST tests were underwater capacitor-discharge-vaporization (CDV) dissassemblies of ~20-g UO_2 samples. These tests were designed to assess the dynamics of the disassembly process, including bubble formation, bubble behavior, and attenuation and transport of the material within the water. The primary variables in these tests were the water pressure and the quantity (pressure) of xenon gas included within the sample. Rapid UO_2 vapor condensation was observed, and insignificant amounts of the UO_2 were transported to the cover-gas region. Pressure oscillations were recorded that are believed to correspond to actual bubble oscillations. The oscillation frequency was observed to increase, as expected, with increasing water pressure.

Five of the six CRI-III tests were intended to establish whether or not the electrical conductivity of UO_2 changes when the UO_2 melts. The results indicate a decrease in electrical conductivity of UO_2 on melting. The remaining CRI-III test was one of a series in which we attempted to use the exposure of motion-picture film as an indicator of sample temperatures during preheat and CDV discharge. This particular test utilized a slower than usual preheat rate to try to prevent motion of the molten fuel

from obscuring the sample viewing region. The slower heating rate did not prove advantageous.

In the secondary-containment nuclear-aerosol studies, results are reported for NSPP test 206 and test 303. Test 304 was also conducted during this reporting period, but the results are not yet available for reporting.

Test 206 was a single-component U_3O_8 aerosol experiment using the plasma-torch aerosol generator in which a concentration of ~10 g/m^3 was achieved.

Test 303 was one of a series of experiments in which U_3O_8 and Na_2O_x aerosols are mixed to study their composite behavior. The results indicate that the two species are coagglomerating and acting together as a mixed-species aerosol. Further evidence for this interactive behavior was obtained in the CRI-II tests, in which we coated the particles with a protective organic polymer before collecting them on grids for viewing and photographing under scanning and transmission electron microscopes. Size distribution measurements and comparisons are also reported for the CRI-II tests using the spiral centrifuge and cascade impactors.

GLOSSARY OF ACRONYMS

ACRR	Annular Core Research Reactor
ART	Aerosol Release and Transport
CDA	core-disruptive accident
CDV	capacitor-discharge vaporization
CRI	Containment Research Installation
FAST	Fuel Aerosol Simulant Test
HCDA	hypothetical core-disruptive accident
LMFBR	Liquid-Metal Fast Breeder Reactor
NRC	Nuclear Regulatory Commission
NSPP	Nuclear Safety Pilot Plant
ORNL	Oak Ridge National Laboratory

LMFBR AEROSOL RELEASE AND TRANSPORT PROGRAM QUARTERLY PROGRESS REPORT FOR JULY–SEPTEMBER 1979

T. S. Kress

ABSTRACT

This report summarizes progress for the Liquid-Metal Fast Breeder Reactor (LMFBR) Aerosol Release and Transport program sponsored by the Division of Reactor Safety Research of the Nuclear Regulatory Commission for the period July–September 1979. Topics discussed include (1) recent capacitor-discharge-vaporization (CDV) tests in the Fuel Aerosol Simulant Test facility conducted under water to evaluate the disassembly process including bubble dynamics and UO_2 vapor condensation and transport; (2) tests in the CRI-III vessel to evaluate UO_2 temperatures during melting and CDV discharge; (3) tests in the CRI-III vessel to establish UO_2 electrical conductivity changes on melting; (4) single-component U_3O_8 aerosol experiments and two-component (U_3O_8 and Na_2O_x) mixed-aerosol experiments in the Nuclear Safety Pilot Plant; (5) experiments in CRI-II using mixed aerosols (U_3O_8 and NO_2O_x), in which attempts are made to coat the particles of the mixed aerosol, to preserve the characteristics for scanning electron microscope and transmission electron microscope photographs; and (6) comparisons of mixed-aerosol size-distribution measurements using a spiral centrifuge and a cascade impactor.

Keywords: aerosol, hypothetical accident, LMFBR fission product release, fission product transport, exreactor experiment, safety, radionuclide transfer.

---

1. INTRODUCTION

The Liquid-Metal Fast Breeder Reactor (LMFBR) Aerosol Release and Transport (ART) Program at Oak Ridge National Laboratory (ORNL), sponsored by the Division of Reactor Safety Research of the Nuclear Regulatory Commission (NRC), is an LMFBR safety program concerned with radionuclide release and transport. Its scope includes (1) radionuclide release from fuel, (2) transport to and release from primary containment boundaries, and (3) behavior within containments. The overall goal of the program is to provide the analytical methods and experimental data necessary to assess the quantity and transient behavior of radionuclides released from LMFBR cores as a result of postulated events of varying

severity up to and including severe hypothetical core-disruptive accidents (HCDAs).

The program is divided into several related experimental and analytical activities:

1. development of a capacitor-discharge-vaporization (CDV) system for deposition of energy in simulated LMFBR fuel (UO_2) that will provide a nonnuclear means for studying the fuel reponse to HCDA-like energy depositions;
2. study of fuel interactions, expansion, and thermal behavior within the sodium pool as the resultant fuel vapor bubble is produced and transported through the sodium to the cover-gas region;
3. development of alternative means for generating fuel-simulant aerosols on a relatively continuous basis;
4. study of the characteristics and behavior of fuel-simulant aerosols in several small vessels;
5. production and study of fuel-simulant and sodium aerosols in the Nuclear Safety Pilot Plant (NSPP) for the validation of models, with particular emphasis on the behavior of mixtures of the two nuclear-aerosol species.

Varying levels of effort are anticipated within these categories, with analytical modeling accompanying the experimental work. The analytical requirements fall into three categories: (1) fuel response to high rates of energy deposition, (2) fuel-bubble dynamic behavior and transport characteristics under sodium, and (3) dynamic aerosol behavior at high concentrations in the bubble and containment atmospheres.

An attempt will be made to consolidate the analyses and data and to present them in a manner that will facilitate direct assessment of the radiological hazard associated with arbitrary hypothetical accident scenarios.

2. EXPERIMENTAL PROGRAM

2.1 Source Term and Simmer Verification Experiments in FAST/CRI-III

A. L. Wright A. M. Smith
J. M. Rochelle

2.1.1 Introduction

The Fuel Aerosol Simulant Tests (FAST) and the CRI-III tests are performed by using the capacitor-discharge-vaporization (CDV) technique to place uranium dioxide fuel samples into the high-energy states that typify LMFBR hypothetical core-disruptive accident levels. The primary goals of the FAST/CRI-III test program are to (1) use the experimental results as a base for developing analytical models that could then be used to predict fuel transport through the coolant in accidents and (2) perform experiments in support of the program to verify models in the Los Alamos Scientific Laboratory SIMMER computer code.

During this quarter 13 tests were performed in the FAST/CRI-III facility, including 7 tests in the FAST vessel and 6 tests in the CRI-III vessel. These tests were of the following types:

1. a "preheat" test (CDV 82) performed in a vacuum environment as part of the "Sandia Normalization" test effort;
2. five "heat-through-melt" tests (CDV 83 through 87) in which the level of preheat was such that none of the pellets was expected to melt and the fuel then would be heated through melt during the capacitor-discharge phase;
3. seven underwater tests in the FAST vessel (FAST 22 through 27 and FAST 29).

Data for the 13 tests are presented in Tables 1 through 3. Individual test results and conclusions are presented in Sects. 2.1.2, 2.1.3, and 2.1.4.

Table 1. Sample data

Test	Pellet stack mass (g)	Pellet stack length (cm)	Microsphere mass (g)	Quartz tube Dimensions ID (cm)	OD (cm)
FAST 22	17.59	9.15	31.06	0.972	1.66
FAST 23	17.72	9.22	30.86	0.972	1.67
FAST 24	17.63	9.16	30.41	0.971	1.66
FAST 25	17.55	9.11	31.06	0.970	1.65
FAST 26	17.54	9.12	31.80	0.970	1.66
FAST 27	17.89	9.29	30.28	0.969	1.65
FAST 29	17.68	9.19	31.98	0.972	1.65
CDV 82	21.73	10.08	35.43	0.970	1.61
CDV 83	17.84	9.28	31.36	0.968	1.66
CDV 84	17.60	9.15	31.46	0.970	1.63
CDV 85	17.75	9.23	31.38	0.972	1.66
CDV 86	18.04	9.37	31.73	0.973	1.67
CDV 87	17.70	9.19	32.51	0.973	1.64

Table 2. High preheat, CDV charging data[a]

Test	High preheat power (W)	Sample resistance after high preheat (Ω)	Number of capacitor banks charged	Charging voltage (V)	Initial bank energy (kJ)
FAST 22	1700	0.45	4	1940	75
FAST 23	1700	0.44	4	1950	75
FAST 24	1700	0.43	4	1950	75
FAST 25	1700	0.[illegible]	4	1950	75
FAST 26	1275	0.[illegible]	4	1950	75
FAST 27	1275	0.78	4	1950	75
FAST 29	1700	0.50	4	1940	75
CDV 82	[b]	[b]	[b]	[b]	[b]
CDV 83	1200	0.91	5	1750	75
CDV 84	1000	1.5	5	1750	75
CDV 85	900	2.1	5	1745	75
CDV 86	1200	0.91	5	1750	75
CDV 87	1200	0.94	5	1745	75

[a]For the FAST experiments high preheat was performed for 28 s, and there was a 2-s time delay between preheat and capacitor discharge. The preheat schedules for the CRI-III tests are discussed in the text.

[b]This was a preheat test; no capacitor discharge was performed.

Table 3. Energy input, aerosol yield data

Test	CDV time to arcing (ms)	CDV energy input to arcing (kJ)	Estimated initial[a] aerosol conc. ($\mu g/cm^3$)	Estimated initial[a] aerosol mass (g)
FAST 22	3.2	35.7	0	0
FAST 23	2.97	36.5	0	0
FAST 24	2.0	23.4	0	0
FAST 25	3.0	35.2	0	0
FAST 26	4.88	42.2	0	0
FAST 27	3.42	31.7	0	0
FAST 29	3.08	32.6	0	0
CDV 82	[b]	[b]	[b]	[b]
CDV 83	5.20	37.5	4.76	2.67
CDV 84	4.34	21.7	2.86	1.60
CDV 85	4.88	19.6	1.83	1.02
CDV 86	10.16	61.5	12.23	6.85
CDV 87	4.48	35.0	5.76	3.23

[a] For FAST experiments aerosol sampling was performed in the argon gas space above the water. The aerosols formed in the CRI-III tests filled the vessel volume (0.56 m^3).

[b] This was a preheat test; capacitor discharge was not performed.

2.1.2 Results from CDV 82 — preheat test performed in a vacuum environment

A series of experiments, designated the "Sandia Normalization" tests, performed at low vessel pressure (~100 μm Hg) in CRI-III, were completed last quarter. In a number of these tests the debris produced by vaporization after capacitor discharge was sampled using a spinning wheel collector developed at Sandia Laboratory. Posttest evaluation of the wheel's contents will permit determination of droplet sizes and velocities produced. The goal of the tests is to compare the debris produced by electrical (CDV) energy with that produced at comparable neutron energy levels in Sandia's Annular Core Research Reactor (ACRR).

For these comparisons, it would be desirable to know the fuel temperature distributions after preheat and during capacitor discharge. The temperature measurements give an independent indication of the fuel energy levels produced and can be compared with calculations using models developed in the ART program. A photographic method, described in the previous quarterly report,[1] is being tried for making these measurements.

Normally, microspheres surround the entire fuel pellet stack in the test assembly. To permit "viewing" of a portion of the pellets, the sample configuration shown in Fig. 1 was used in a number of the previously performed tests. Using this configuration, we had hoped to measure the pellet surface and center temperatures.

In one of the preheat tests, CDV 78, we attempted to measure fuel pellet temperatures during the final ("high") preheat stage and during sample cooldown after high preheat. Observations of the motion pictures indicated bright flashes at the pellet surface that were probably due to motion of the molten fuel. This apparent fuel motion disturbed the fuel pellet surface as well as the hole in the pellet and made reliable temperature measurements impossible.

The high preheat stage (at ~2200 W) usually follows a period at 500 W. We felt that the flashes in CDV 78 might have been due to the abruptness of the change from 500- to 2200-W heating. In CDV 82 a different heating schedule was used. After the 500-W heating, the sample was heated at 1000 W for 20 s, then 1600 W for 20 s, and finally at 2200 W for 28 s. The sample configuration shown in Fig. 1 was again used, and motion pictures were taken at 200 frames per second starting at the end of the 500-W heating stage. Again bright flashes were observed in the motion pictures made during the 2200-W heating stage. This result seems to indicate that the fuel motion was not due to the abruptness of the increase in power to the sample, but was due simply to the level of power. Calculations indicate that fuel pellet melting should occur at 2200 W.

More tests in the Sandia Normalization series are planned for January 1980. In these, a different fuel pellet viewing configuration will be tried in an attempt to achieve accurate temperature measurements.

2.1.3 Discussion of results from heat-through-melt tests performed in CRI-III

Measurements made by Kim et al.[2] indicate a large increase (perhaps a factor of 3) in the thermal conductivity of UO_2 on melting. Different mechanisms have been hypothesized for such a conductivity increase, but as yet there is no agreement as to which mechanism actually causes it. However, phenomena that cause an increase in thermal conductivity may

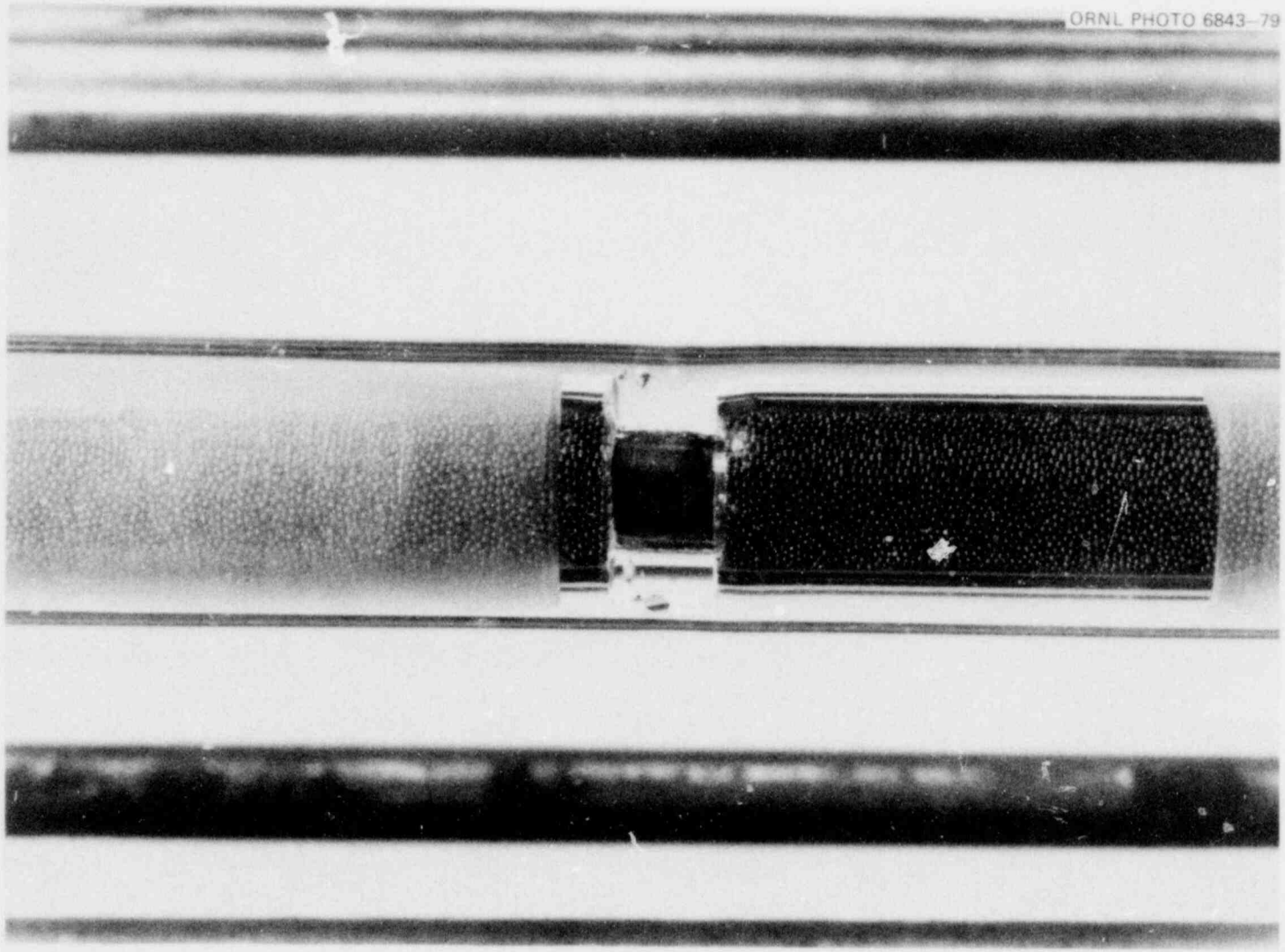

Fig. 1. Close-up of test assembly used in CDV 82. Shown is an exposed UO_2 pellet with a 0.16-cm-diam (1/16-in.) hole bored to its center. Also shown are UO_2 microspheres surrounding the remainder of the pellet stack.

also cause a change (either increase or decrease depending on the mechanism) in the electrical conductivity. We have been asked[3] if there were any experiments we could perform with our CDV system that would permit at least a qualitative judgment of UO_2 electrical conductivity changes as fuel is heated through melt. Such experiments could provide some insight as to which mechanisms may be responsible for the increase in thermal conductivity.

Standard test procedure in the capacitor discharge experiments is to perform high preheat at a level at which the pellets are essentially all molten before capacitor discharge (this level was determined by sectioning samples after preheat had been performed in some of the early CDV tests). In the tests discussed here (CDV 83 through 87), preheat levels used were such that the fuel was not expected to be melted after preheat. By evaluation of the capacitor discharge voltage and current data, then, we hoped to determine whether or not there had been a change in electrical conductivity as the UO_2 passed through the melt stages.

CDV 83. The high preheat level for this test was 1200 W, which was maintained for 38 s. Data from the capacitor-discharge phase are presented in Figs. 2, 3, and 4. As shown in Fig. 3, the discharge current rises (because of fuel heating and the accompanying decrease in sample resistance), then becomes almost constant for a short time, and at ~2.92 ms after the start of discharge decreases by ~20% over a short time period.

Figure 4 shows the measured overall sample resistance vs time for CDV 83. Corresponding to the 20% current decrease at 2.92 ms, the resistance increases by ~20%. After this abrupt increase in resistance, which occurred over a 0.1-ms time period, the resistance then decreased as a function of time until 5.2 ms, when the sample breakup occurred.

CDV 84. High preheat was performed at 1000 W for 43 s; this power level was lower than that used in CDV 83. As shown in Fig. 5, an ~20% decrease in capacitor discharge current occurred at 3.78 ms after the start of discharge. Sample breakup occurred shortly after the current decrease. Measurements indicated that the aerosol yield produced in CDV 84 was less than that produced in CDV 83 (see Table 3).

CDV 85. High preheat was performed at 900 W for 38 s. An ~50% decrease in discharge current (corresponding to an ~50% sample resistance

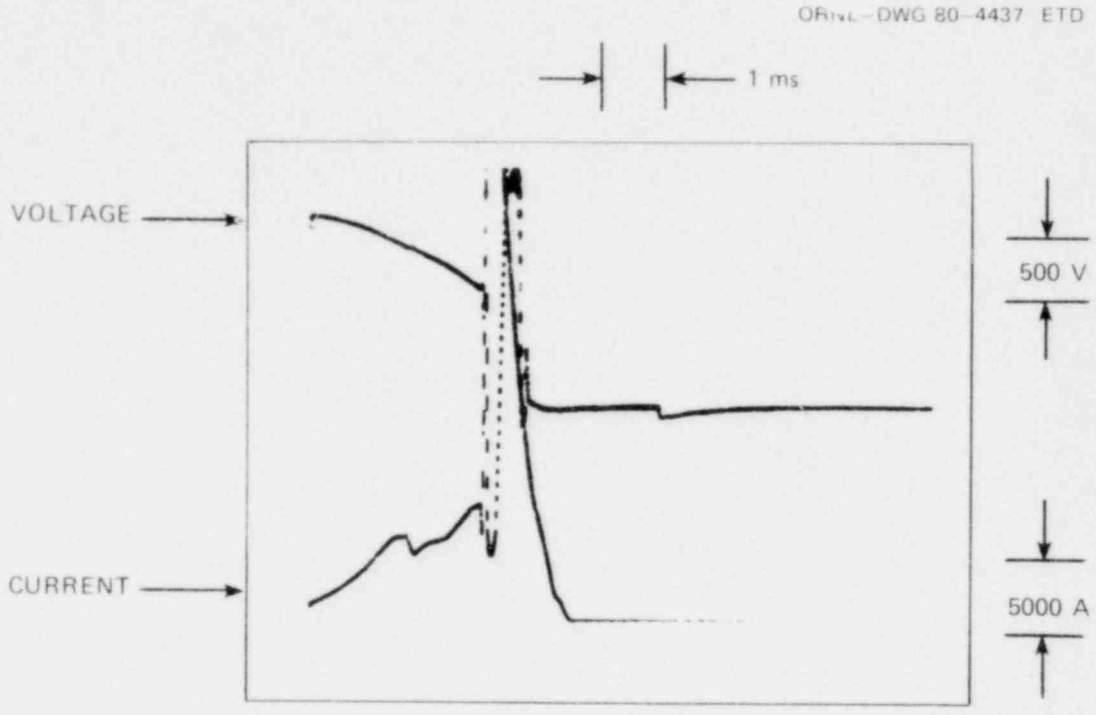

Fig. 2. Oscilloscope recording of voltage and current data from CDV 83 (500 V/Division, 5000 A/Division, 1 ms/Division).

Fig. 3. Expanded view of current data from CDV 83. Current at 2.92 ms after capacitor discharge is ~1.33 V × (5000 A/V) = 6650 A.

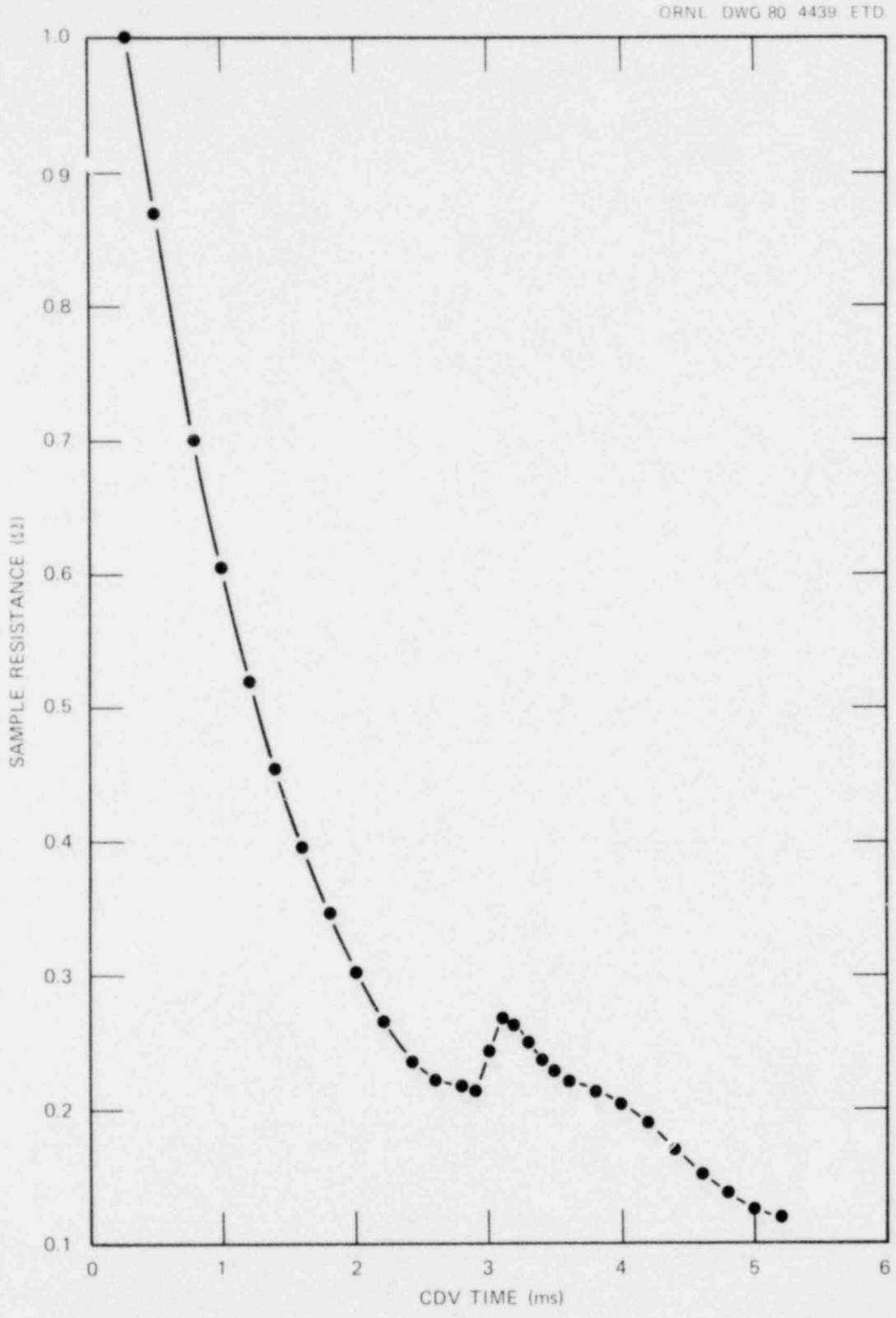

Fig. 4. Fuel sample resistance vs time during capacitor discharge for CDV 83.

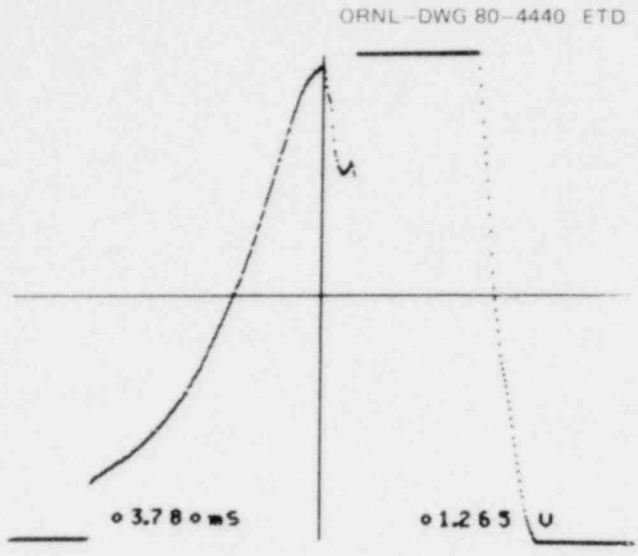

Fig. 5. Expanded view of current data from CDV 84. Current at 3.78 ms after capacitor discharge is ~1.265 V × (5000 A/V) = 6325 A.

increase) occurred at ~4.5 ms after the start of capacitor discharge. Sample breakup occurred shortly after 4.5 ms, and the aerosol yield was less than in CDV 83 and 84.

CDV 86. Preheat and capacitor discharge settings for this test were the same as those used in CDV 83. As shown in Fig. 6, up to 5.2 ms after capacitor discharge (when sample breakup occurred in CDV 83), the discharge current results for CDV 86 closely resemble those found for CDV 83. For CDV 86 the capacitor discharge energy input time of 10.12 ms was much longer than the 2- to 5-ms input times that typically occur. Consequently, the 61.5-kJ CDV energy input and the 6.85-g initial aerosol yield are among the highest levels ever produced in the CRI-III tests.

CDV 87. In CDV 83 through 86 a 2-s delay between the end of preheat and the start of capacitor discharge was used. This 2-s delay is normally used in the FAST and CRI-III experiments to try to reduce the temperature gradient across the fuel pellets by allowing heat exchange from the central region to the edges. A reduced gradient should result in a more even deposition of energy to the pellet region during capacitor discharge.

The high preheat level for CDV 87 was 1200 W, the same as for CDV 83 and 86. However, in CDV 87 the 1200-W heating was maintained for 39.6 s,

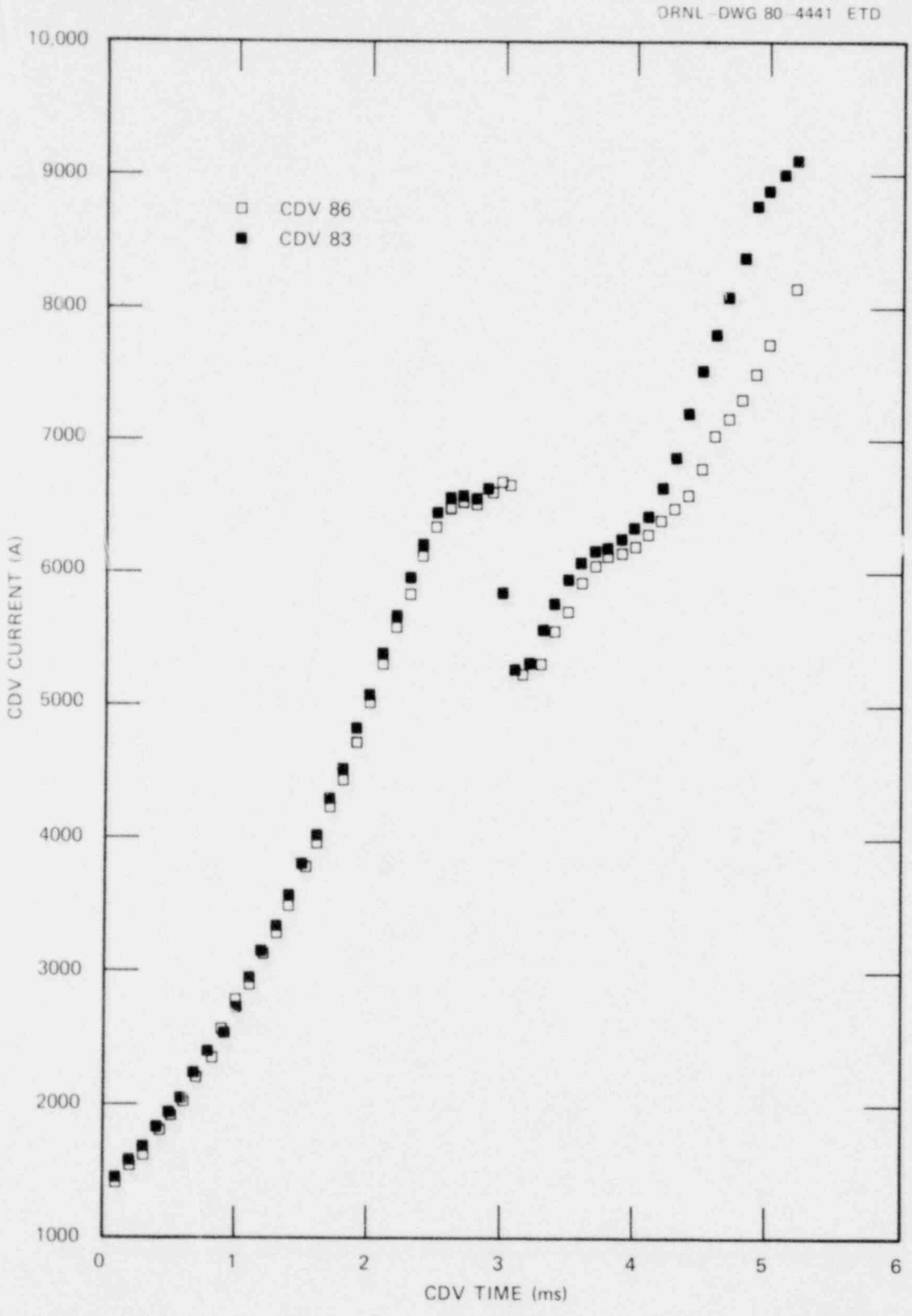

Fig. 6. Capacitor-discharge-current data for CDV 83 and 86.

and the time delay between preheat and capacitor discharge was reduced from the normal 2 s to only 0.4 s.

A comparison of capacitor-discharge-current data for CDV 86 and 87 is shown in Fig. 7. The drop in current occurred at ~2.4 ms in CDV 87, ~0.5 ms earlier than in CDV 86.

Summary of results, with preliminary conclusions. Table 4 summarizes some of the important data from CDV 83 through 87. A number of observations can be made from these data:

1. Decreasing the preheat power before capacitor discharge caused the "CDV time to current drop" to increase.
2. Comparing CDV 83 and 87, reducing the time delay between preheat and capacitor discharge reduced the "CDV time to current drop." Note that the amount of cooling of the fuel during this time delay should decrease as the time delay is shortened.
3. The sample resistance at the time of current reduction was roughly the same for all five tests.

These three observations indicate that the drop in current is due to some unique phenomenon, possibly to a decrease in the electrical conductivity

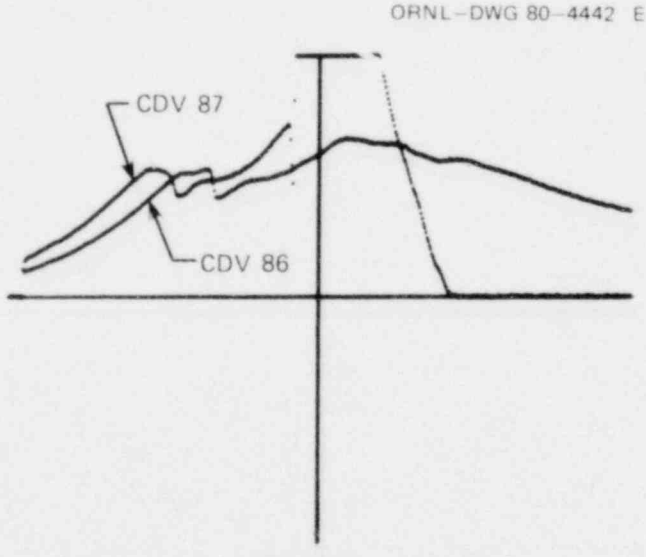

Fig. 7. Capacitor-discharge-current oscilloscope traces for CDV 86 and 87.

Table 4. Selected data from CDV 83 through 87

Test	High preheat power (W)	Time delay between preheat and CDV (s)	CDV time to current drop (ms)	Sample resistance at this time (Ω)
CDV 87	1200	0.4	2.4	0.225
CDV 83	1200	2	2.9	0.215
CDV 86	1200	2	3.06	0.210
CDV 84	1000	2	3.78	0.230
CDV 85	900	2	4.5	0.253

of UO_2 as it is heated through melt. Certainly, there was no indication in the tests of an increase in UO_2 electrical conductivity as it was heated through melt (although if the decreased conductivity was not due to melting, an increase in conductivity could be hidden).

More experiments, as well as detailed test analyses, are needed to conclude confidently that the observed decrease in the overall electrical conductivity in these tests was the result of a real change in the material resistivity.

2.1.4 Discussion of results from FAST water tests

During this quarter seven water tests were performed in the FAST facility. Most of these tests were performed at conditions outlined in the FAST experiment plan.[4] For all tests the water level above the fuel vaporizer unit was 112 cm (44 in.), and the water temperature was ~298 K (73°F). The main parameters varied in the tests were pressure of the argon gas above the water and pressure of the xenon gas trapped inside the vaporizer unit. A summary of these pressure settings is presented in Table 5.

In these tests measurements were made of the pressure pulses produced by bubble expansion and contraction. These were made using a Kaman pressure transducer mounted 22.9 cm (9 in.) from the test sample; signals were recorded for $\geq$80 ms after capacitor discharge. High-speed motion pictures of the tests were also taken. Finally, a few minutes after capacitor discharge the argon gas above the water was sampled to determine if any fuel

Table 5. Value for argon cover-gas pressure, xenon gas pressure in the fuel vaporizer unit used in FAST tests 22 through 27 and 29

Test	Argon pressure [MPa (atm)]	Xenon pressure [MPa (atm)]
FAST 22	0.122 (1.20)	0.135 (1.34)
FAST 23	0.123 (1.22)	0.135 (1.34)
FAST 24	0.122 (1.20)	0.135 (1.34)
FAST 25	0.128 (1.27)	0.513 (5.08)
FAST 26	0.125 (1.24)	0.513 (5.08)
FAST 27	0.128 (1.27)	0.513 (5.08)
FAST 29	1.029 (10.18)	1.063 (10.52)

vapor or aerosol had been transported up through the water during the test.

FAST 22. Preheat and capacitor discharge went smoothly in this test, and a large amount of energy (35.7 kJ) was input into the sample during capacitor discharge. The pressure trace recorded in this test is shown in Fig. 8. The early pulse was due to sample break-up and bubble formation, while the later pulses are due to bubble collapse and rebound. The second pulse was nearly as large as the first, perhaps indicating the occurrence of a small fuel-coolant interaction with resultant water vaporization. No fuel aerosol was found in the argon cover gas after the test

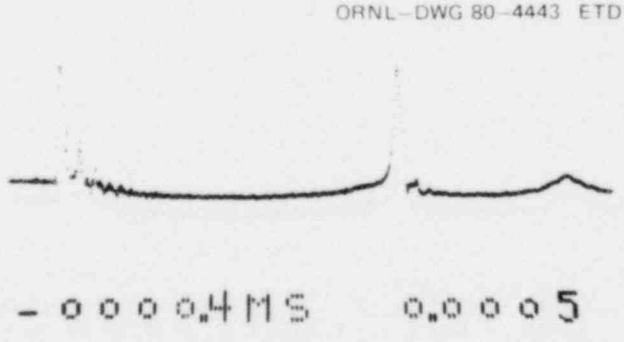

Fig. 8. Recorded pressure vs time data for FAST 22. Pressure pulses occurred at 0.9, 58.3, and 86.8 ms after sample breakup and had magnitudes of 1.45, 1.40, and 0.23 MPa (14.4, 13.9, and 2.2 atm) respectively. Pressure was measured 22.9 cm (9 in.) away from the test sample.

(this result held true for all seven FAST tests described here). The high-speed cameras did not function properly, so no visual record was obtained.

FAST 23. Conditions for this test were the same as for FAST 22. A high input of capacitor discharge energy again occurred. Qualitatively, the pressure history was much like that produced in FAST 22, except that the magnitude of the second pressure pulse was about half that produced in FAST 22. The high-speed cameras ran, taking motion pictures through the side port of the vessel and through a port at the top of the vessel.

FAST 24. Pretest conditions were the same as those in FAST 22 and 23. Though the CDV energy input was somewhat lower than in the previous two tests, the recorded pressure data looked much like that produced in FAST 22 and 23.

FAST 25. The xenon pressure inside the fuel vaporizer unit was increased to 0.513 MPa (5.08 atm), roughly five times the level used in the previous three tests. A high CDV energy input was produced, but the steel tube surrounding the fuel sample did not rupture efficiently. In this test only two pressure pulses (as opposed to three in 23 and 24) were observed during the 80-ms test-recording period.

FAST 26. The argon and xenon gas pressure conditions for this test were the same as those in FAST 25. The vessel interior was lit by shining a high-intensity 2000-W lamp through the top port of the vessel. In previous tests only about 10 ms of the time after sample breakup could be filmed; we hoped this additional lighting would permit more of the experiment to be photographed.

Surprisingly, the CDV electrical data looked much like the data produced in the tests described in Sect. 2.1.3. That is, as shown in Fig. 9, an ~20% drop in current occurred ~2.4 ms after the start of capacitor discharge. After performing FAST 27, we observed that one of the circuit breakers for the sample preheater had been tripped. As a result, instead of a high preheat of 1700 W (which is expected to melt the pellets), the high preheat level for FAST 26 and 27 was 25% less, or 1275 W. In spite of the difference in preheat levels for FAST 25 and 26, the pressure traces for these two tests were similar — only two pulses produced in 80 ms.

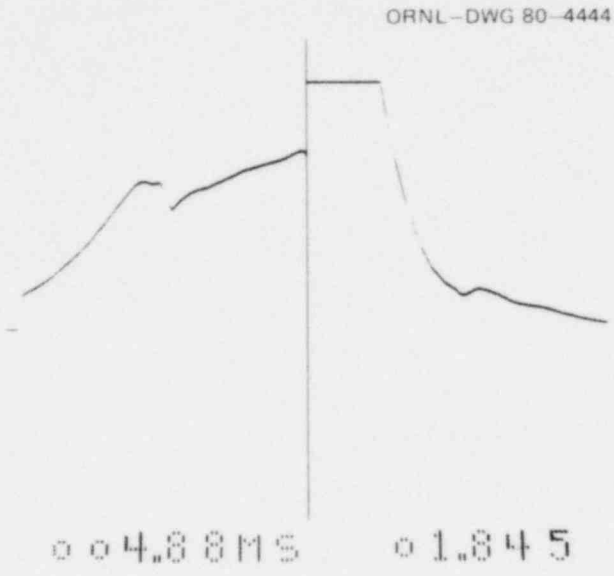

Fig. 9. Oscilloscope trace for capacitor discharge current in FAST 26. Note the sharp reduction in current that occurred ~2.4 ms after the start of capacitor discharge.

FAST 27. Conditions for this test were the same as for FAST 26. Input of capacitor discharge energy was roughly 25% less than in FAST 26, and three pressure pulses were observed during the 80-ms pressure-recording time.

The interior of the vessel was again lit by shining a 2000-W lamp through the top port. For FAST 27 the camera framing rate was 500 frames/s, a factor of 20 less than the usual framing rate. Thus, much more of the experiment could be photographed, and the bubble oscillations were observed for the first time. Film from FAST 27 indicates that the fuel vapor in the bubble rapidly condenses and forms a "fog"; it is this fog that makes it difficult to film the experiments without external lighting.

FAST 29. Before performing tests at ~2.02 MPa (20 atm) argon and xenon pressures, we decided to perform one scoping test at an ~1.01-MPa (10-atm) pressure level (FAST 28 was to have been performed under these conditions but had to be aborted during preheat). Though the CDV energy input level was fairly high (30+ kJ), no loud shock like those produced in FAST 22 through 27 was heard.

As shown in Fig. 10, the pressure history was much different from that produced in the six earlier tests. In particular, the time between the first two pressure pulses was ~5 ms, about ten times less than the periods in FAST 22 through 27. At least ten pressure peaks were produced in the 80-ms recording period. Motion pictures of the test indicated that the bubble produced had a much smaller diameter than those produced in FAST 22 through 27.

Summary of results. Results from high-speed motion pictures indicate that fuel-vapor-bubble condensation in these tests was very rapid, probably occurring in less than 100 ms after the start of bubble formation. In addition, increasing the amount of xenon in the bubble (comparing FAST 22–24 with FAST 25–27) did not significantly change the bubble behavior. This may indicate that bubble condensation is not diffusion-controlled (and so not influenced by the xenon level), but that condensation occurs by some other mechanism (perhaps radiation heat loss or coolant entrainment). Measurements in the argon cover gas indicate that an insignificant amount of the UO_2 was transported through the water by the xenon gas bubble that should have been left after fuel condensation.

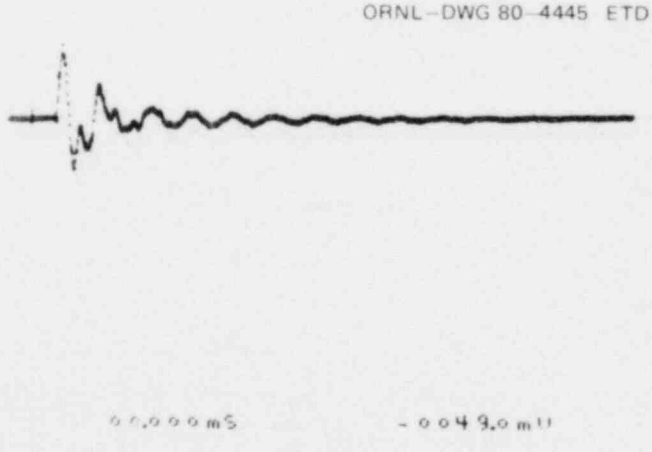

Fig. 10. Recorded pressure vs time data for FAST 29; data recorded for ~80 ms after the start of capacitor discharge. The first pressure peak occurred 0.88 ms after sample breakup and had a magnitude of 1.89 MPa (18.8 atm). Pressure was measured 22.9 cm (9 in.) away from the test sample.

Pressure measurement results are summarized in Table 6. These results indicate that

1. variations in energy level had little influence on the magnitude of the first pulse produced;
2. increasing the argon pressure (FAST 29) reduced the time between pressure pulses (as expected, because of reduced bubble size);
3. increasing the amount of xenon in the bubble seems to increase the time between pressure events (again expected, because for a fixed fuel energy, increased xenon pressure means increased bubble size);
4. the large second pressure pulses in FAST 22 and 26 may be due to small-scale fuel-coolant interactions.

2.2 Secondary Containment Aerosol Studies in the NSPP

R. E. Adams J. T. Han

2.2.1 Introduction

Activities of the NSPP during this period included (1) analysis of data from the third uranium oxide aerosol test (test 206), which used the plasma-torch aerosol generator; (2) performance of the first mixed-oxide aerosol test (test 303) and analysis of resulting data; and (3) performance of the second mixed-oxide aerosol test (test 304).

2.2.2 Uranium oxide aerosol test No. 206

This test was the third and last of the test series to study the performance of the plasma-torch uranium oxide aerosol generator.[5] The powder feeder was charged with 1 kg (2.2 lb) of uranium metal powder. This material was injected into the plasma-torch combustion chamber over a 5-min period. The vessel atmosphere was air at a relative humidity of less than 20%, and the initial pressure and temperature were ambient. Duration of the test was 48 h.

Aerosol mass concentration. By extrapolating the data obtained from the filter samplers and by using data from the fallout and plateout samplers, we estimated a maximum aerosol concentration of 10 g/m^3. Average aerosol concentration values as a function of time are displayed in Fig. 11.

Table 6. Data for time of peak pressure (after start of sample breakup); P = peak pressure for first three pulses produced in FAST 22–27 and FAST 29

Test	Time (ms)	~P[a] [MPa (atm)]
	First pulse	
FAST 22	0.9	1.45 (14.4)
FAST 23	1.09	1.28 (12.7)
FAST 24	0.92	1.43 (14.2)
FAST 25	0.98	1.25 (12.4)
FAST 26	1.12	1.06 (10.5)
FAST 27	1.12	1.38 (13.7)
FAST 29	0.88	1.89 (18.8)
	Second pulse	
FAST 22	58.3	1.40 (13.9)
FAST 23	49.2	0.52 (5.1)
FAST 24	49.0	0.27 (2.7)
FAST 25	52.0	0.26 (2.6)
FAST 26	55.1	0.71 (7.0)
FAST 27	46.5	0.32 (3.2)
FAST 29	5.9	1.39 (13.8)
	Third pulse	
FAST 22	86.8	0.23 (2.2)
FAST 23	68	0.25 (2.5)
FAST 24	66	0.18 (1.8)
FAST 25	[b]	[b]
FAST 26	[b]	[b]
FAST 27	66.5	0.16 (1.6)
FAST 29	12.7	1.15 (11.4)

[a] Argon cover-gas pressure in FAST 22–27 was ~0.12 MPa (1.2 atm); argon cover-gas pressure in FAST 29 was ~1.03 MPa (10.2 atm).

[b] Third pulse not observed in 80-ms pressure recording time.

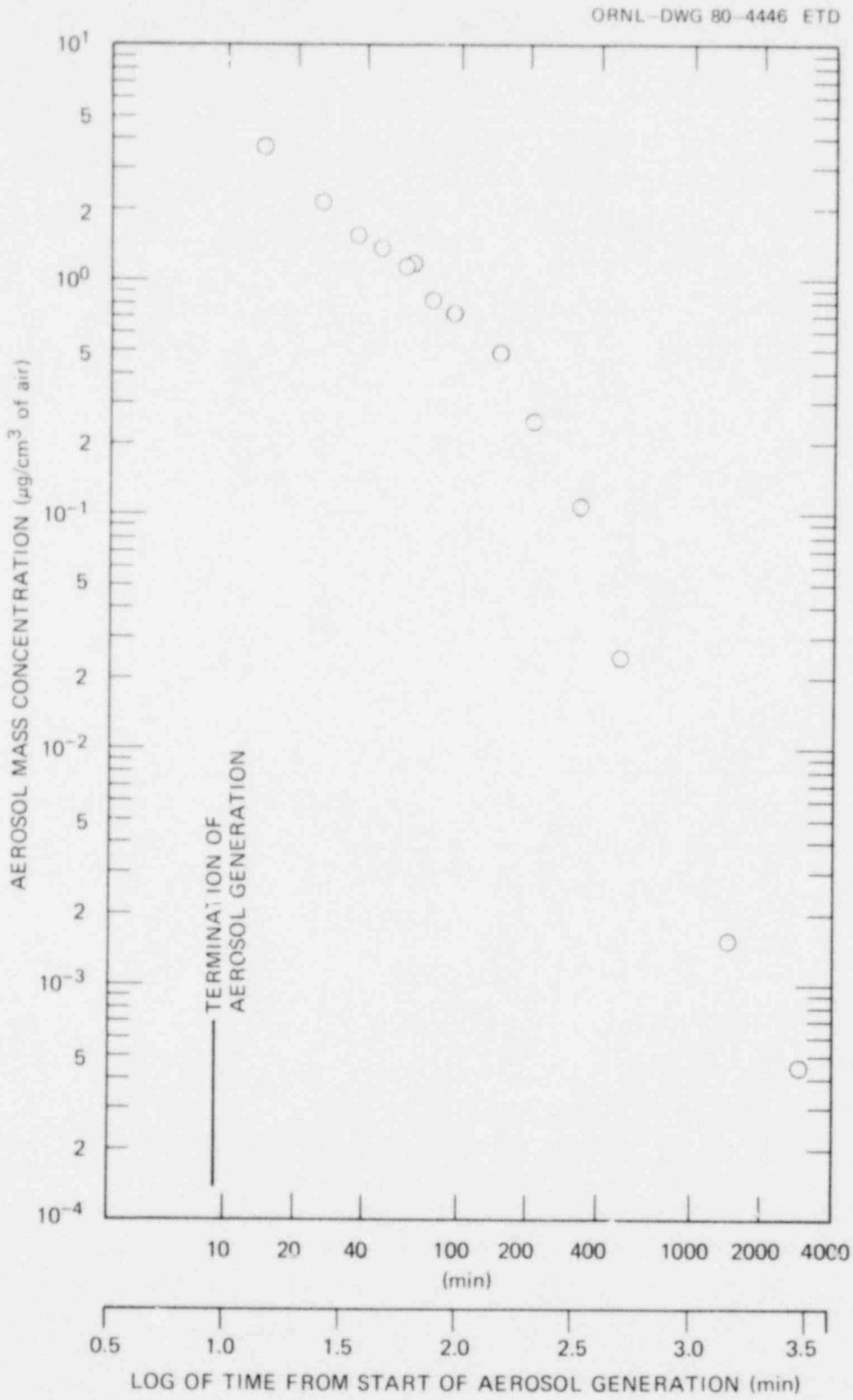

Fig. 11. Average aerosol mass concentration – test 206.

Aerosol particle size. The aerodynamic mass mean diameter of the aerosol was measured over the first 8.4 h of the test. Six aerosol samples were taken with an eight-stage cascade impactor (Andersen Mark III). Results are given in Table 7.

Table 7. Uranium oxide aerosol particle size — test 206

Sample No.	Time after start of aerosol generation (min)	Aerodynamic mass mean diameter (μm)	Geometric standard deviation (σ_g)
1	17	3.2	3.4
2	38.5	3.3	2.3
3	81	3.3	2.3
4	190	3.0	1.9
5	345	2.3	1.9
6	504	2.3	1.9

Distribution of aerosol. At the termination of the test, the approximate distribution of aerosol, as determined by the fallout and plateout samplers, was as follows: (1) aerosol settled onto floor, 65%; (2) aerosol plated onto interior surfaces, 35%; and (3) aerosol still suspended in the vessel atmosphere, nil.

2.2.3 Mixed uranium–sodium oxide aerosol test No. 303

This test was the first in which the two aerosols were generated simultaneously. The target mixed-oxide aerosol concentration was 20 g/m^3, composed of equal masses of uranium oxide and sodium oxide. Uranium oxide aerosol generation (with the plasma-torch generator) was initiated first and then followed by sodium oxide generation (by a sodium pool fire) 1.5 min later. The uranium oxide aerosol generation period was approximately 25 min, and the sodium oxide aerosol generation period was approximately 12 min. The vessel atmosphere was air at a relative humidity of less than 20%, and the initial pressure and temperature were ambient. Test duration was 119 h.

Aerosol mass concentration. Three min after termination of aerosol generation the first measurement was made of the aerosol mass concentration. Total aerosol mass concentration at that time was 2.51 g/m^3 composed of 1.40 g/m^3 of uranium oxide and 1.11 g/m^3 of sodium oxide. Aerosol mass concentrations for each component of the aerosol as a function of time are given in Fig. 12. The concentration values for sodium oxide at times longer than 300 min are probably slightly higher than actual values. The reagents used in dissolving the mixed-oxide sample were found to have low-level sodium impurities; the reported data were corrected to compensate for this reagent contamination.

Based upon extrapolation of the aerosol concentration data and upon fallout and plateout data, we concluded that the target total aerosol mass concentration was approached. Over the first 6 h of the test, the measured mass ratio of uranium oxide to sodium oxide ranged from 1:3 to 2:5. According to this preliminary analysis of the results of this test, apparently the two aerosols were coagglomerating, and the composite behavior was somewhat different from that of a single-component aerosol in that the initial rate of disappearance from the vessel's atmosphere was greater.

Aerosol particle size. The aerodynamic mass median diameter of the aerosol was measured over the first 9.8 h; a sample taken at 24 h did not contain sufficient material for proper analysis. The aerosol material from each collector plate of the impactor was analyzed for both uranium and sodium content. If the two aerosols are coagglomerated, one would expect that the particle diameter as determined by using the uranium or sodium content of the total mass, or the total mass, would be similar. Table 8 contains the calculated diameter for each component as well as for the total mass. Except for the first sample, the diameter calculated for each component and the diameter calculated for the total mass are similar, lending further evidence that the two aerosols are coagglomerating.

Distribution of aerosol. At the termination of the test (119 h), the approximate distribution of the aerosol components, as determined by the fallout and plateout samplers, was as follows: (1) aerosol settled onto floor of vessel, 88% (sodium oxide) and 82% (uranium oxide); (2) aerosol plated onto internal surfaces, 12% (sodium oxide) and 18% (uranium oxide); (3) aerosol still suspended in the vessel atmosphere, nil.

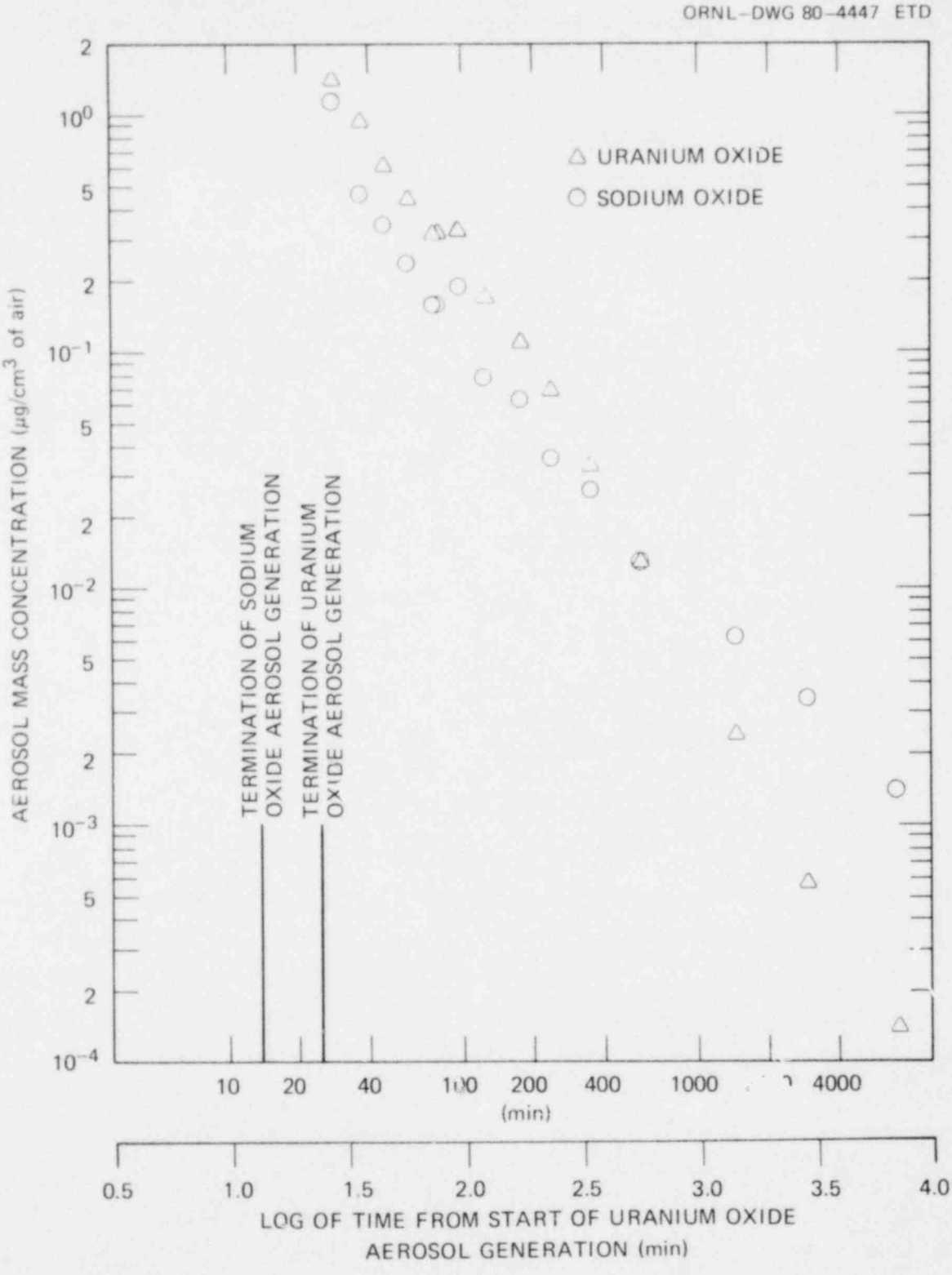

Fig. 12. Average aerosol mass concentration — test 303.

Table 8. Mixed uranium oxide–sodium oxide aerosol particle size – test 303

Sample No.	Time[a] (min)	AMMD calculated by using: Uranium oxide component AMMD[b] (μm)	Uranium oxide component σg[c]	Sodium oxide component AMMD (μm)	Sodium oxide component σg	Total aerosol mass AMMD (μm)	Total aerosol mass σg
1	31	3.8	3.6	5.6	4.3	4.0	3.6
2	55	3.4	3.4	3.2	5.0	3.2	3.5
3	100	3.0	2.4	2.7	3.4	2.9	2.5
4	205	2.4	2.6	1.8	4.0	2.3	2.7
5	360	1.9	2.5	0.8	5.0	1.5	2.9
6	590	1.6	2.3	1.1	4.6	1.4	2.7

[a]Time after start of uranium oxide aerosol generation.

[b]Aerodynamic mass median diameter.

[c]Geometric standard deviation.

2.2.4 Mixed uranium–sodium oxide aerosol test No. 304

The second mixed-aerosol test in which the aerosols were generated simultaneously was performed late in this reporting period, and complete results are not available from the analytical laboratory. The test was performed in a manner similar to that of test 303, and the target total mass concentration was 20 g/m^3 with a 10:1 ratio of uranium oxide to sodium oxide.

2.3 Basic Aerosol Experiments in CRI-II

G. W. Parker A. L. Sutton, Jr.

2.3.1 First mixed-oxide aerosol characterization test

The first of a continuing series of mixed-aerosol (U_3O_8-Na_2O_2) characterization tests was completed in the CRI-II facility as a preliminary

to the NSPP series of large-scale tests. This run is designated Mixed-Oxide Run PT-28. Previous work on characterizing LMFBR fuel–sodium aerosols has been reported by Allen and Bryant[6] from Battelle Northwest Laboratories (BNWL). Their technique, however, induced a somewhat unique aerosol because the metallic sodium was first condensed onto the fuel (PuO_2-UO_2) oxide particle; the sodium then ignited. Even so, in dry air, they observed no compound formation; but with higher humidity sodium uranyl tricarbonate was formed. Because of the relatively low concentration of their experiments, the maximum aerodynamic size observed was only about 0.8 μm.

In our experiments the aerosol mixture is generated by simultaneously burning powdered uranium in a metal-oxygen torch and spraying hot liquid sodium into dry air with spontaneous ignition. Thus, the oxides are independently formed, then condensed and mixed by strong thermal convection forces. The ratio of uranium oxide to sodium peroxide was to have been about 1:1; however, it actually reached about 3.2 parts uranium oxide to 1 part sodium peroxide, which remained constant during most of the settling period. The initial sampling was somewhat delayed for pressure adjustment because of excessive heating and cooling. The longer time than usual to adjust the pressure to 1 atm was due to an undersized air supply valve, which has since been replaced. (The pressure and temperature transients are shown in Fig. 13.)

The maximum initial aerosol concentration was not accurately determinable because of the time delay; however, we estimate that it was between 10 and 20 g/m^3 based on total settled aerosol and the limited sampling data shown in Fig. 14.

2.3.2 Size distribution of U_3O_8 and Na_2O_2 by spiral centrifuge and cascade impactor analyses

Although our spiral centrifuge was known to have developed some instability, the cause of which had not been determined, the instrument was used nonetheless; the collected foils from this mixed-oxide experiment appeared to be uniform and relatively consistent with the pure sodium peroxide distributions previously observed. The uniform deposits on the

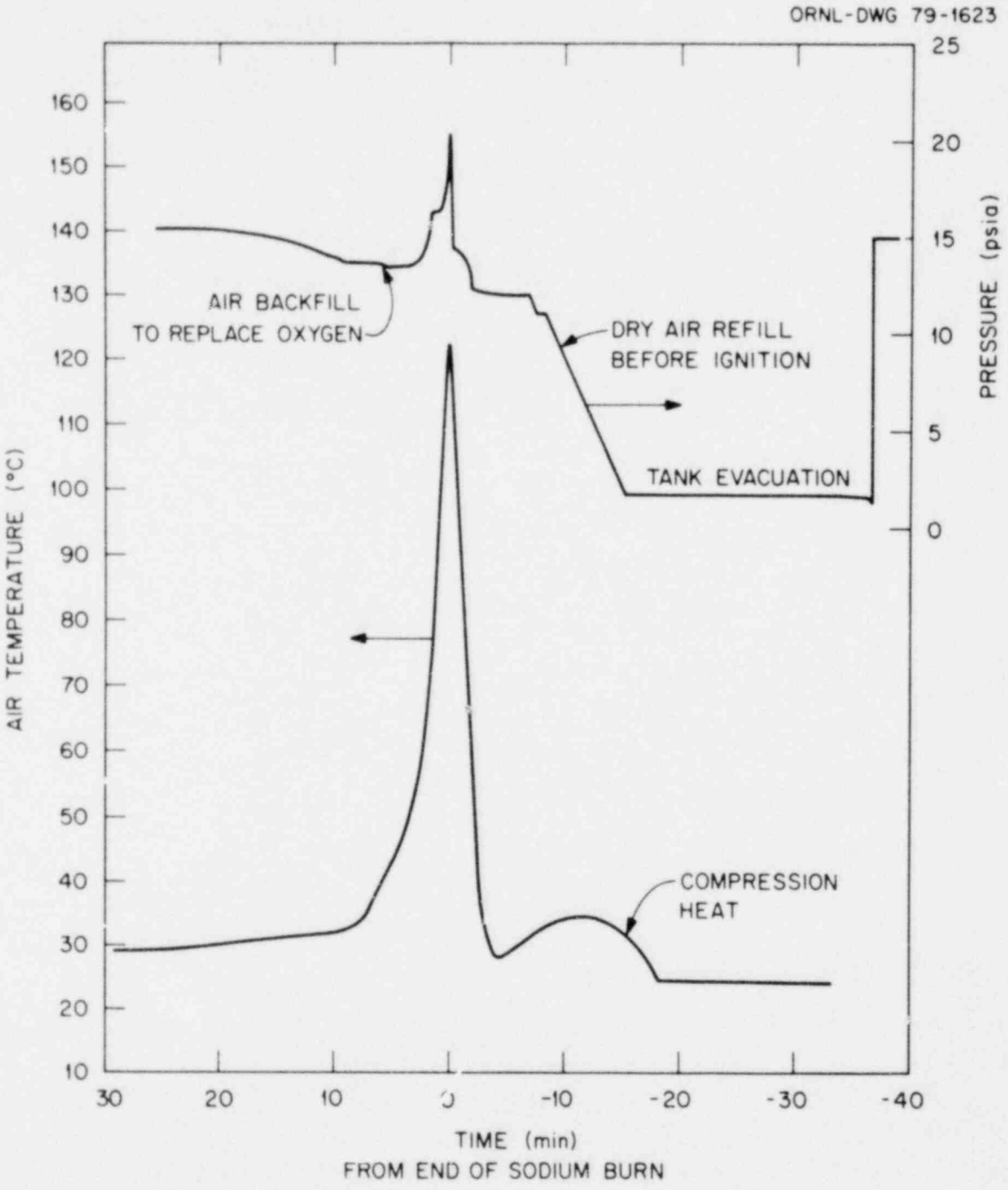

Fig. 13. Pressure-temperature curve for burning operation for mixed-oxide run PT-28.

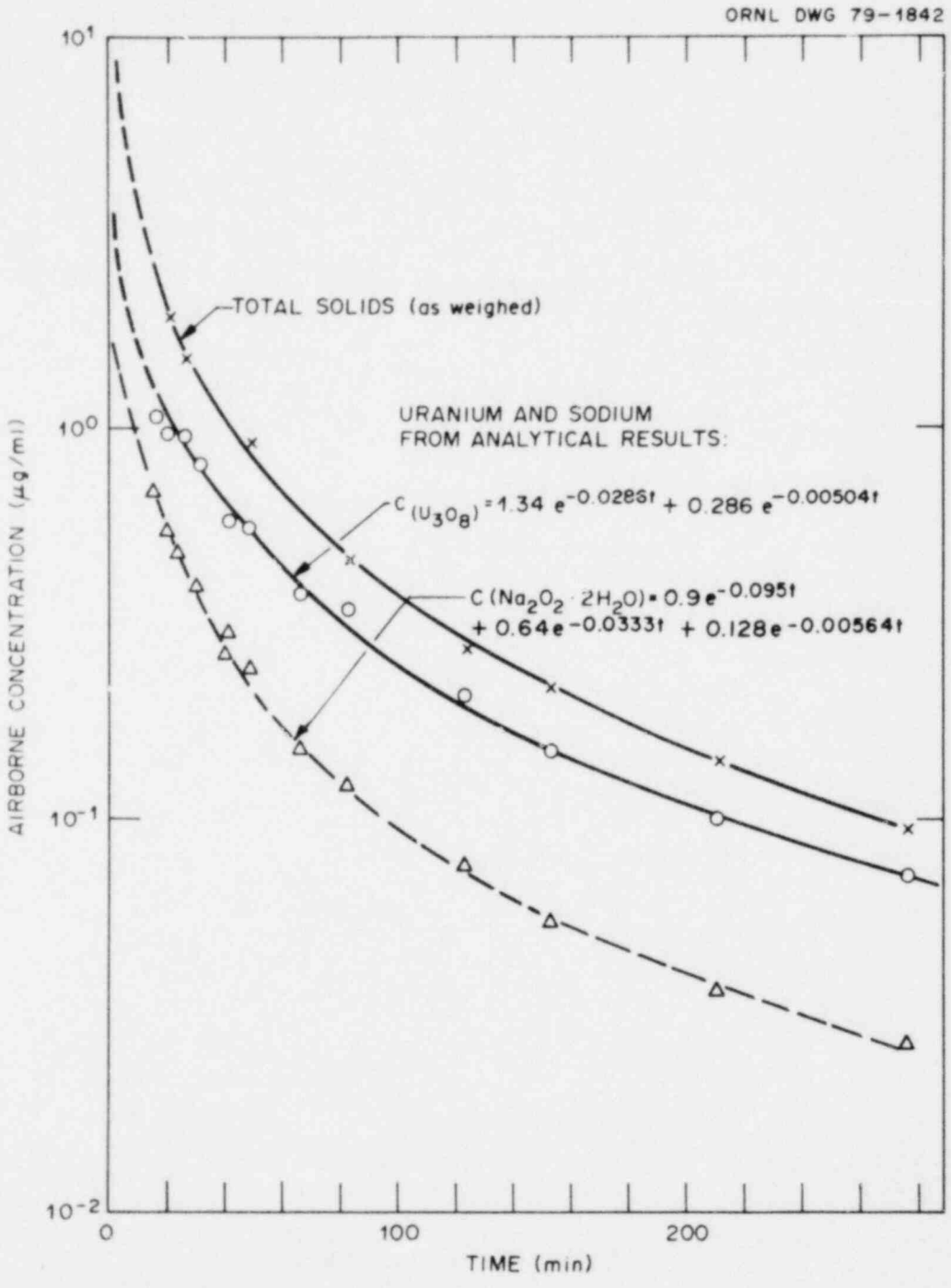

Fig. 14. Rate of deposition curves for mixed-oxide run PT-28.

foils are shown in Fig. 15, and the graphic form of the analytical data is shown in Fig. 16.

An Andersen eight-stage cascade impactor was also operated to take three samples each with the original "large cut" first and second stages and with the new redesigned stages. The first, second, and fourth rows in the photograph in Fig. 17 show the new stages having the smaller number of jets on the first two plates. The improvement in matching the spiral centrifuge measurements by using the new stages can be seen in Table 9 and in Figs. 18 and 19, which show only the data taken with the new stages.

Table 9. Summary of size distribution measurements

Elapsed time (min)		Uranium		Sodium	
		D_{50} (μm)	GSD (σ)	D_{50} (μm)	GSD (σ)
19	1st Cent. (3000 rpm)	3.97	1.34	4.41	1.40
22	Imp. No. 1 (new stages)	3.43	1.84	3.86	2.27
61	Imp. No. 2 (new stages)	3.46	1.82	3.86	2.20
107	Imp. No. 3 (old stages)	3.19	1.74	3.19	1.93
203	2nd Cent. (3000 rpm)	3.83	1.35	5.26	1.42
231	Imp. No. 4 (new stages)	3.46	1.82	3.56	2.08
256	3rd Cent. (3000 rpm)	3.56	1.35	4.78	1.41
287	Imp. No. 5 (old stages)	2.68	1.69	2.82	2.13
352	Imp. No. 6 (old stages)	2.77	1.7	3.06	1.97

2.3.3 Photomicrographic display of mixed-oxide aerosols

Several earlier attempts to photograph primary particles of sodium peroxide on microscope grids generally have given unsatisfactory results because atmospheric moisture has destroyed the original features of the spherical sodium-compound aggregates. By first depositing a protective organic polymer coating over the particles before collecting on grids, we have produced relatively well-defined particle photographs by both the SEM and TEM techniques. The two types of photographs shown at different

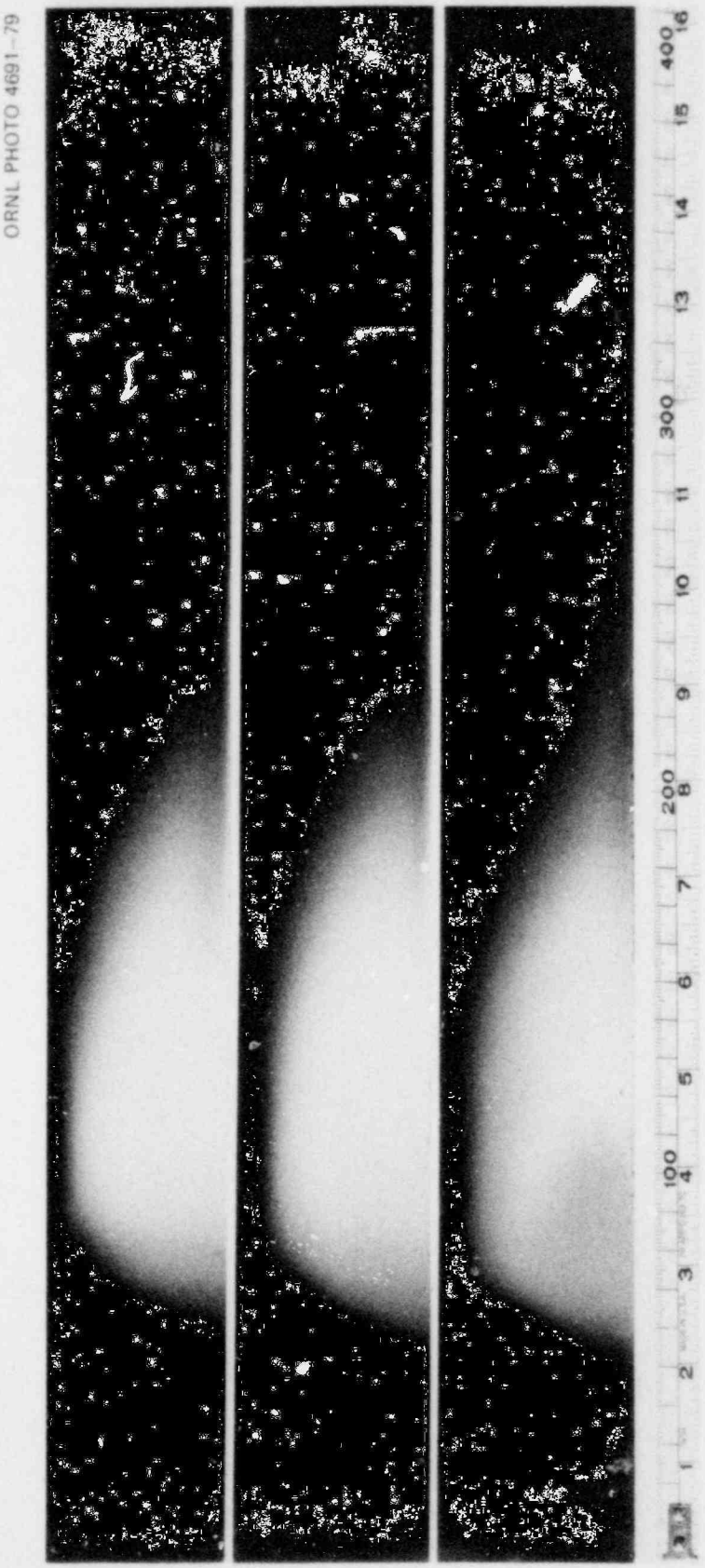

Fig. 15. Centrifuge foils from mixed-oxide run PT-28.

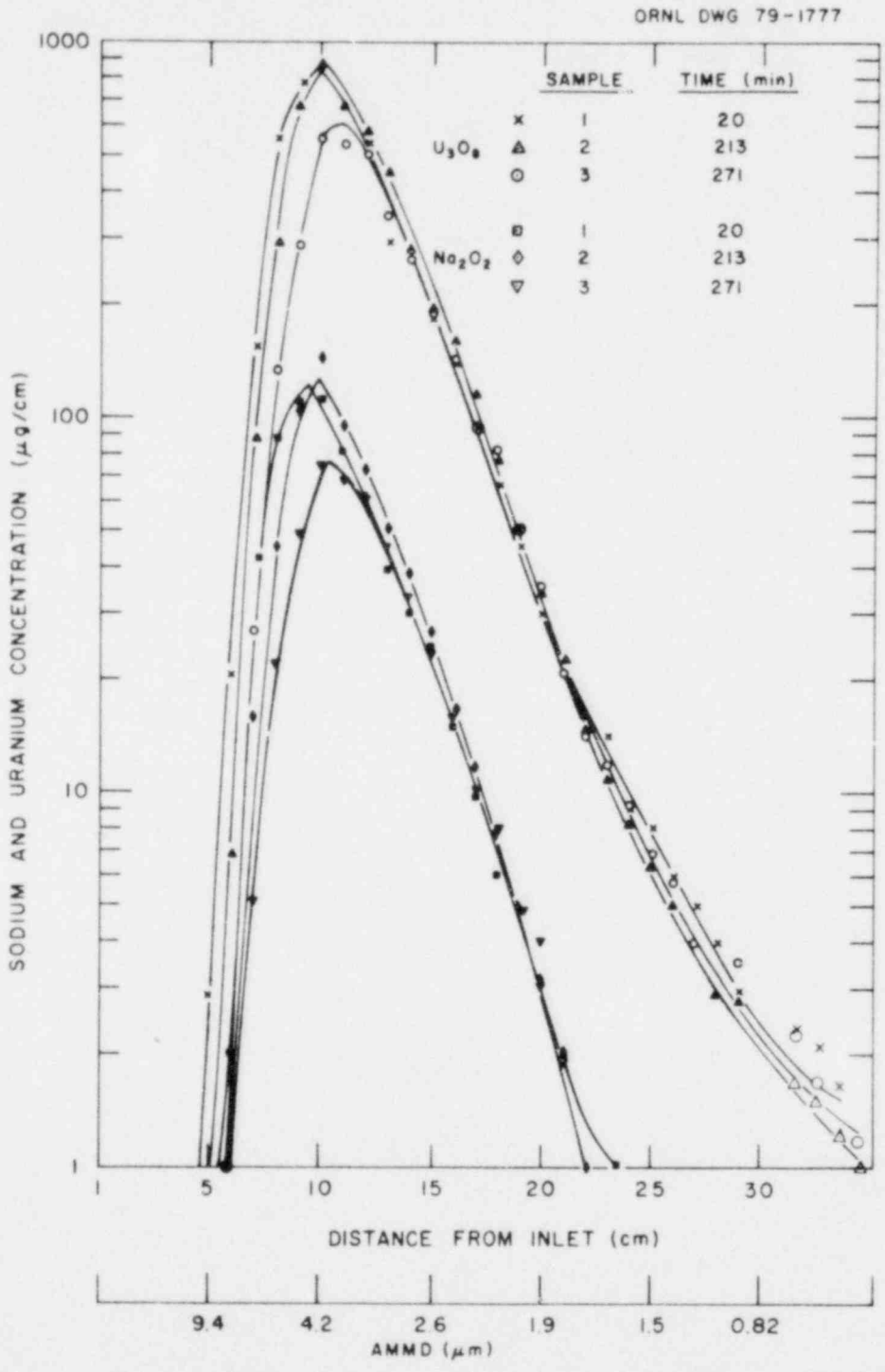

Fig. 16. Spiral centrifuge size distributions for sodium and uranium oxide in mixed-oxide run PT-28.

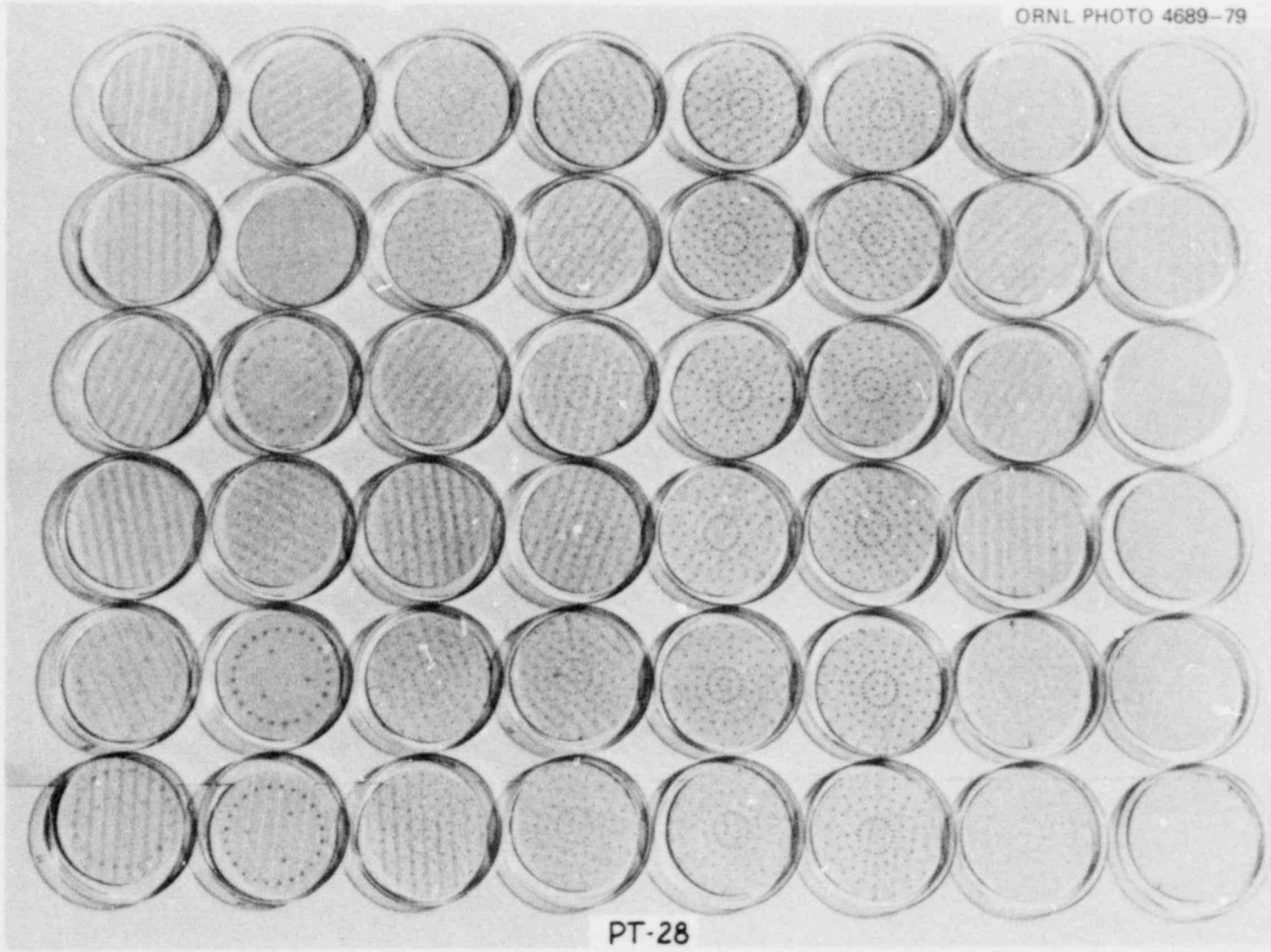

Fig. 17. Impactor collector plates for run PT-28.

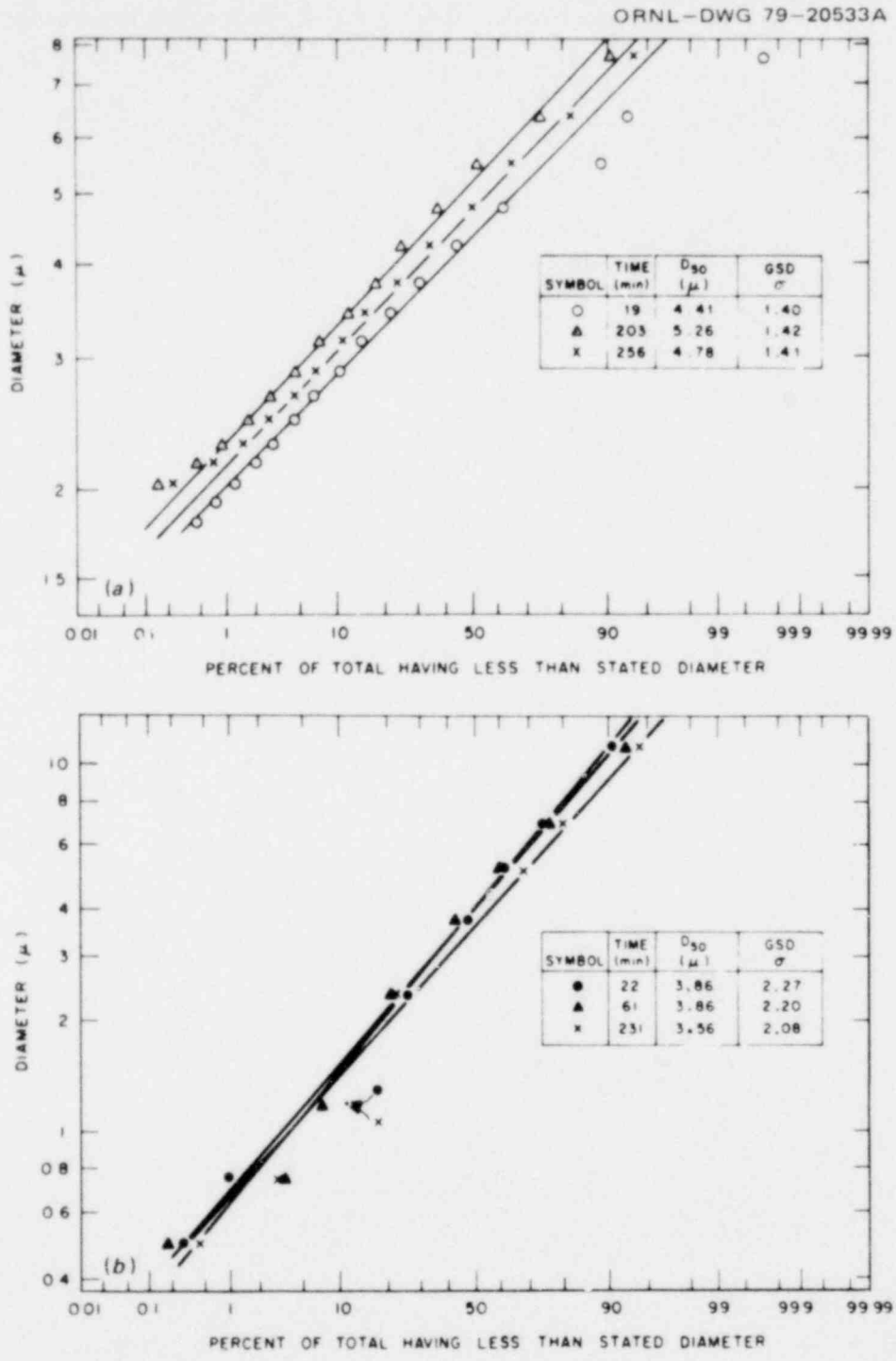

Fig. 18. Sodium oxide size distributions for mixed-oxide run PT-28: (a) spiral centrifuge samples; (b) impactor samples with new stages 0 and 1.

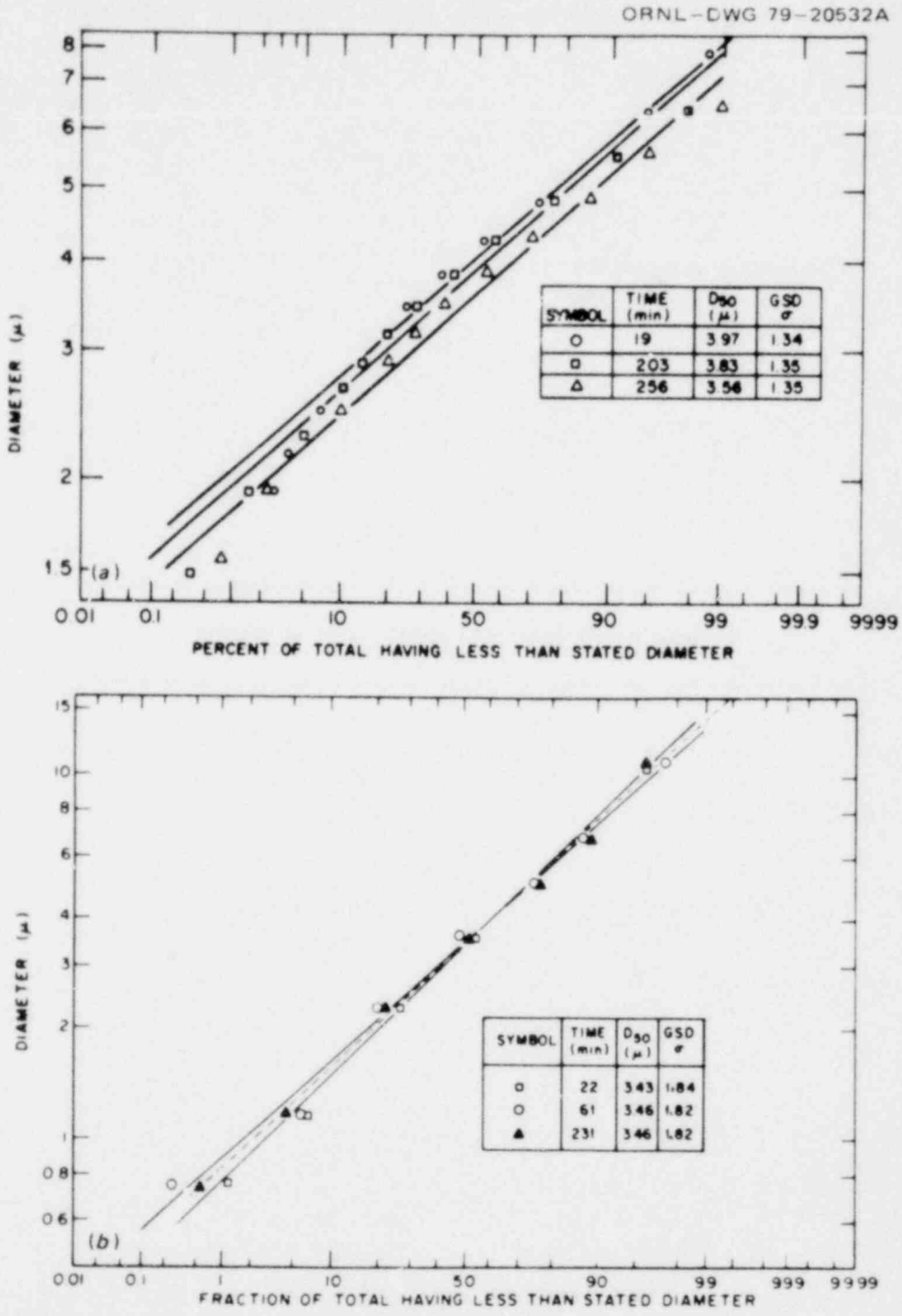

Fig. 19. Uranium oxide size distributions or mixed-oxide run PT-28: (a) spiral centrifuge samples; (b) impactor samples with new stages 0 and 1.

magnifications are seen in Figs. 20 and 21. The small chain-like aggregates are U_3O_8, while the large spheres resembling popcorn balls are sodium peroxide. They appear to be coagglomerated, as is indicated by the constant symmetrical size distributions in Fig. 16. In the larger magnifications the sodium seems to encapsulate large numbers of U_3O_8 primary particles.

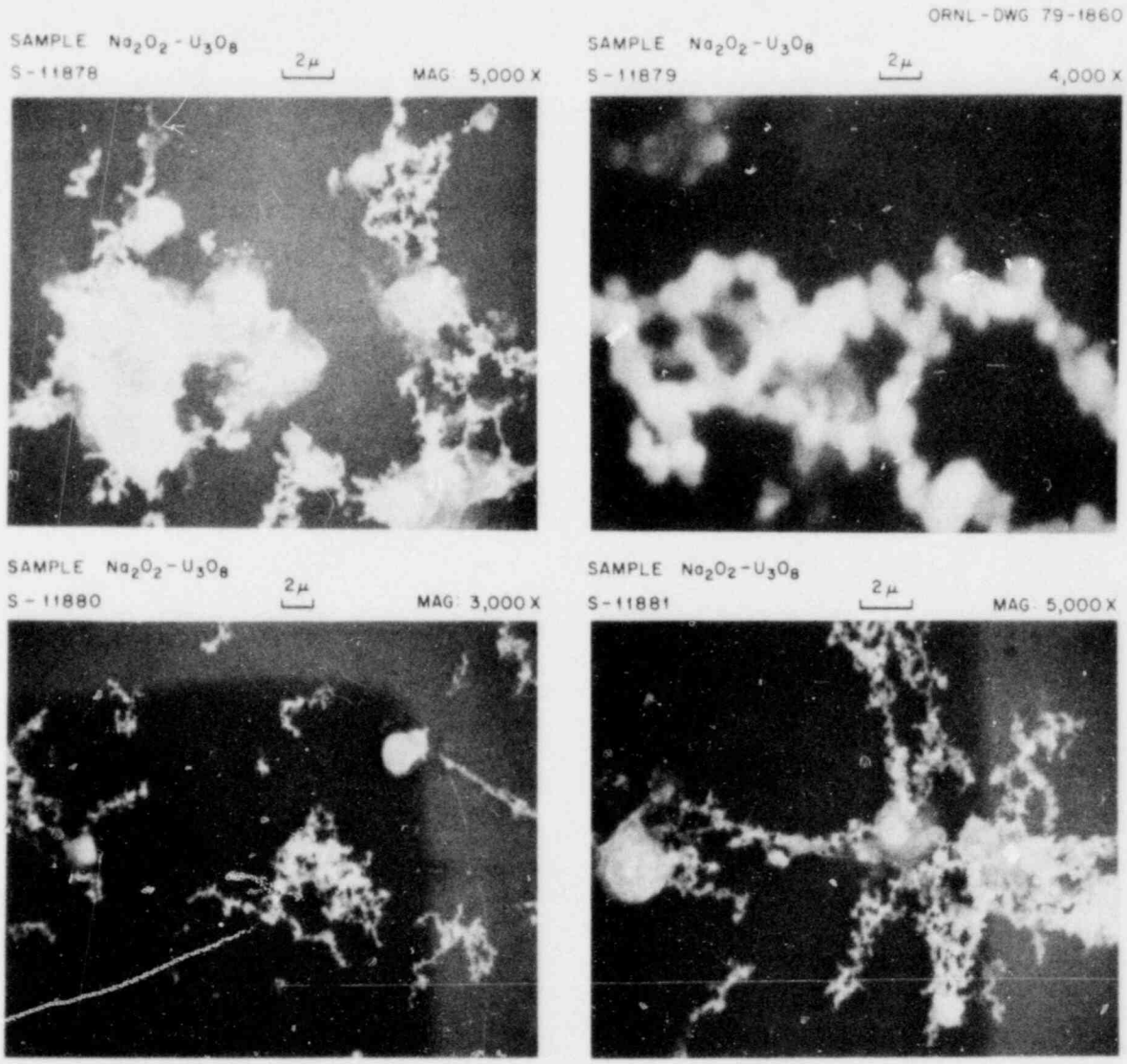

MIXED URANIUM OXIDE – SODIUM PEROXIDE PARTICLES
AFTER COATING WITH ORGANIC POLYMER

Fig. 20. SEM photomicrograph for mixed-oxide run PT-28. (Original reduced 15.5%)

ORNL-DWG 79-1861

T-342 PT-28 MIXED OXIDES 1 cm = 0.26 μm 37,000 X

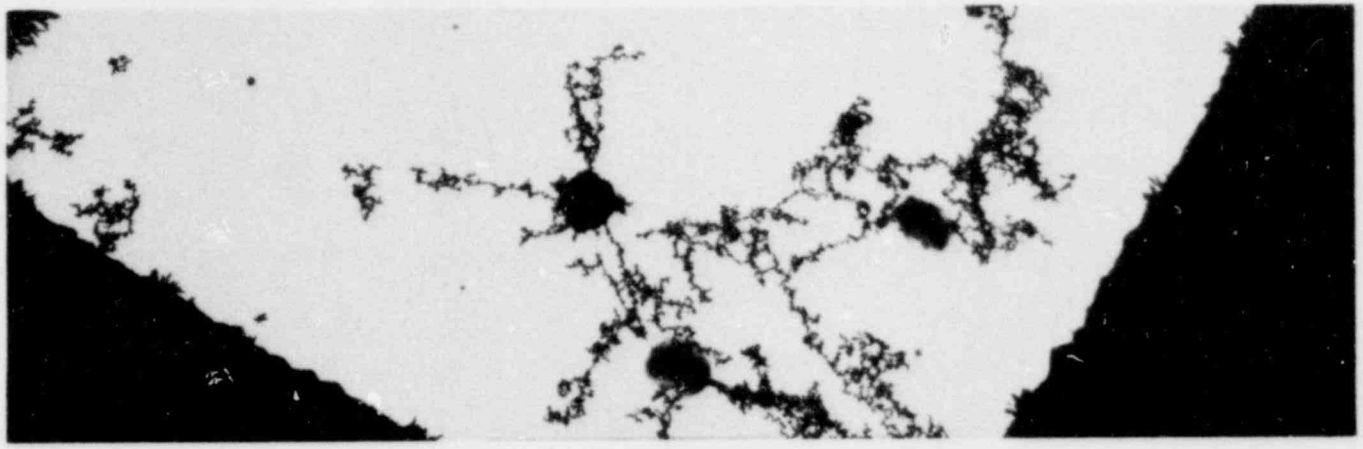

T-334 PT-28 MIXED OXIDES 1 cm = 2.9 μm 3,700 X

Fig. 21. TEM photomicrograph for mixed-oxide run PT-28. (Original reduced 20%)

In the succeeding tests, which will cover a range of concentrations and sodium-to-uranium ratios, we hope additional data will confirm the precision of the centrifuge aerodynamic size measurements and the relative accuracy of the impactor analysis, including that from a new Sierra rectangular jet unit such as is used at the Containment Systems Test Facility (CSTF).[7] Additional data will be derived to establish more exactly the chemical composition and evidence of any compound formation between the oxides.

3. ANALYTICAL PROGRAM

Efforts are continuing to develop computerized models for source-mitigating phenomena that are speculated to occur as high-energy molten fuel expands, flash vaporizes, and, in general, thermally interacts with the coolant (sodium or water). Presently, these models include condensation due to convective and radiant heat transfer to the bubble/coolant interface (including the presence of noncondensable gases) and conduction heat transfer into the coolant. Models are also being developed for condensation onto structure and onto entrained coolant. Models being developed at the University of Virginia for use in this program include particle fragmentation, aerosol nucleation, and bubble dynamics and condensation during the early phases of bubble development, including bubble oscillations, coolant entrainment, and vapor condensation.

Efforts are also being made to develop appropriate averaging techniques for the properties of two component mixtures of nuclear aerosols that can be used in the computerized analytical models developed to describe the behavior of single-component aerosols.

REFERENCES

1. T. S. Kress and A. L. Wright, *LMFBR Aerosol Release and Transport Program Quarterly Progress Report for April–June 1979*, ORNL/NUREG/TM-354 (to be published).

2. C. S. Kim et al., "Measurement of Thermal Diffusivity of Molten UO_2," 7th Symposium on Thermophysical Properties, National Bureau of Standards, Gaithersburg, Md., 1977.

3. Paul Abrahamson, Argonne National Laboratory, personal communication.

4. A. L. Wright and A. M. Smith, *Updated Work Plan for the FAST/CRI-III Fuel Vaporization and Transport Experiments*, ORNL/NUREG/TM-326 (October 1979).

5. T. S. Kress and J. T. Han, *LMFBR Aerosol Release and Transport Program Quarterly Progress Report for January–March 1979*, ORNL/NUREG/TM-329 (August 1979).

6. M. D. Allen and R. K Bryant, "Characterization of LMFBR Fuel-Sodium Aerosols," *Health Phys.* 35, 237–54 (1979).

7. R. K. Hilliard et al., "Sodium Oxide/Hydroxide Aerosol Properties and Behavior in a Large Vessel," pp. 764–91 in *Proceedings of the 15th DOE Nuclear Air Cleaning Conference, August 7–10, 1978, Boston, Massachusetts*, ed. by Melvin W. First, CONF-780819, NTIS, Springfield, Va., 1979.

NUREG/CR-1296
ORNL/NUREG/TM-376
Dist. Category R7

Internal Distribution

1. R. E. Adams
2. M. Bender
3. H. W. Bertini
4. J. R. Buchanan
5. W. B. Cottrell
6. G. F. Flanagan
7-8. M. H. Fontana
9. J. T. Han
10. H. W. Hoffman
11-13. T. S. Kress
14. Milton Levenson
15. R. E. MacPherson
16. A. P. Malinauskas
17. F. R. Mynatt
18. G. W. Parker
19. P. Patriarca
20-21. J. L. Rich
22. J. M. Rochelle
23. A. M. Smith
24. I. Spiewak
25. A. L. Sutton, Jr.
26. D. G. Thomas
27. M. L. Tobias
28. H. E. Trammell
29. D. B. Trauger
30. J. L. Wantland
31. J. A. Stevens
32. R. P. Wichner
33. G. D. Whitman
34-36. A. L. Wright
37. ORNL Patent Office
38-39. Central Research Library
40. Y-12 Document Reference Section
41-42. Laboratory Records Department
43. Laboratory Records (RC)

External Distribution

44. D. L. Basdekas, Experimental Fast Reactor Safety Research Branch, Division of Reactor Safety Research, Nuclear Regulatory Commission, Washington, DC 20555
45. M. S. Berberg, Chief, Experimental Fast Reactor Safety Branch, Division of Reactor Safety Research, Nuclear Regulatory Commission, Washington, DC 20555
46-49. Director, Office of Nuclear Regulatory Research, Nuclear Regulatory Commission, Washington, DC 20555
50. Office of Assistant Manager, Energy Research and Development, DOE, ORO
51-52. Technical Information Center, DOE
53-412. Given distribution as shown in category R7 (NTIS-10)

☆ U.S. GOVERNMENT PRINTING OFFICE: 1980-640-245-459